GEOLOGICA CARPATHICA, AUGUST 2011, 62, 4, 299–307 doi: 10.2478/v10096-011-0023-x

Peri-Amazonian provenance of the Central Dobrogea terrane (Romania) attested by U/Pb detrital zircon age patterns

ION BALINTONI[1*], CONSTANTIN BALICA[1,3], ANTONETA SEGHEDI[2] and MIHAI DUCEA[3]

[1]Department of Geology, Faculty of Biology and Geology, "Babeş-Bolyai" University, M. Kogălniceanu Str.1, 400084 Cluj-Napoca, Romania; *ioan.balintoni@ubbcluj.ro
[2]National Institute of Marine Geology and Geoecology, Dimitrie Onciul Str., 23–25 Bucharest, Romania
[3]Department of Geosciences, University of Arizona, Gould-Simpson, Tucson AZ, 85721, USA

(Manuscript received May 6, 2010; accepted in revised form March 17, 2011)

Abstract: The Central Dobrogea Shield is a part of the Moesia, a Paleozoic composite terrane located southward of the North Dobrogea Alpine orogen. The two geological units are separated from each other by a trans-lithospheric discontinuity, the Peceneaga-Camena transform fault. Along this fault, remnants of a Variscan orogen (i.e. North Dobrogea), recycled during the Alpine orogeny come in contact with two lithological entities of the Central Dobrogea Shield, unaffected by the Phanerozoic orogenic events: the Histria Formation, a flysch-like sequence of Ediacaran age very low-grade metamorphosed and its basement, the medium-grade metamorphosed Altîn Tepe sequence. Southward, along the reverse hidden Palazu fault, the Histria Formation meets South Dobrogea, formed of quite different geological formations. Detrital zircon from the Histria Formation yielded U/Pb LA ICP MS ages that show provenance patterns typical of peri-Amazonian terranes. Such terranes were sourced by orogens ranging from Paleoarchean to Neoproterozoic. The ages between 750 and 600 Ma differentiate the Amazonian sources from the Baltican and Laurentian sources, since they are lacking from the last ones. The youngest ages of 587 and 584 Ma suggest for the Histria Formation a maximum late Ediacaran deposition age. At the same time, the continuity of the Ordovician sediments over the Palazu fault revealed by drill-cores favours a Cambrian junction between Central and South Dobrogea.

Key words: peri-Amazonian provenance, Central Dobrogea, terrane analysis, detrital zircon ages.

Introduction

Moesia is a major structural unit of the Carpathian and Balkan foreland. It lies at the SE margin of the East European craton (Fig. 1, inset), in the SE part of the Trans-European Suture Zone (TESZ), a fundamental terrane boundary separating the Precambrian craton from the cluster of terranes originating from Gondwana (e.g. Pharaoh 1999; Yanev et al. 2005; Oczlon et al. 2007). Inspite of the great progress in knowledge of the litho- and biostratigraphy of the Moesian platform cover, the pre-Mesozoic paleocontinental affinity of Moesia is still poorly known, due to the scarcity of reliable geochronological and provenance data. Classically, Moesia was regarded as a southern margin of Baltica (Ziegler 1986). Correlations with the Avalonian terranes were proposed by Matte et al. (1990) and von Raumer et al. (2002, 2003). Other reconstructions relate the Moesia terrane to Gondwana-derived terranes of the Armorican Terrane Assemblage (ATA) (Pharaoh 1999; Golonka 2002). On the basis of various available types of data Oczlon et al. (2007) conclude that Moesia contains four distinct terranes, two of Avalonian (Central and South Dobrogea) and two of Baltican (West Moesia and Palazu) origin, juxtaposed during a long history of Paleozoic and Mesozoic strike-slip displacements.

According to Żelaźniewicz et al. (2009) Brunovistulia, Małopolska and Moesia formed at the end of the Neoproterozoic the Teisseyre-Tornquist Terrane Assemblage (TTA), a mixture of crustal elements derived from both Gondwana and Baltica. Central and South Dobrogea are cited as fragments of Baltican origin. Such different opinions make it difficult to understand the real geological history of southeast Europe. For solving the terrane provenance issue, either paleomagnetic, paleontological, sedimentological approaches or other can be used. Yet, especially in the case of the metamorphosed pre-Alpine basement, or in that of Precambrian sequences, the detrital zircon age patterns become of crucial importance (e.g. Nance & Murphy 1996; Fernández-Suárez et al. 2002; Linnemann et al. 2004, 2007; Samson et al. 2005; Zulauf et al. 2007; Kuznetsov et al. 2010). In order to establish the provenance of Central Dobrogea, we sampled for detrital zircon the very low-grade metasediments of the Histria Formation, which covers this area on large surfaces. The zircons were dated by U/Pb LA-ICP-MS method at University of Arizona, Tucson, and the resulting data are the subject of this article.

Geological setting

Moesia

Moesia, called the Euxinic craton by Balintoni (1997), represents a continental block of ca. 600 km long (east-west) and 250–300 km broad (north-south), located on the present territories of Romania and Bulgaria (Fig. 1, upper-left inset). According to Balintoni (1997) it consists of the Central Dobrogea Shield where the basement crops out on large surfaces and the Moesian platform where the basement is covered by thick Phanerozoic sedimentary deposits.

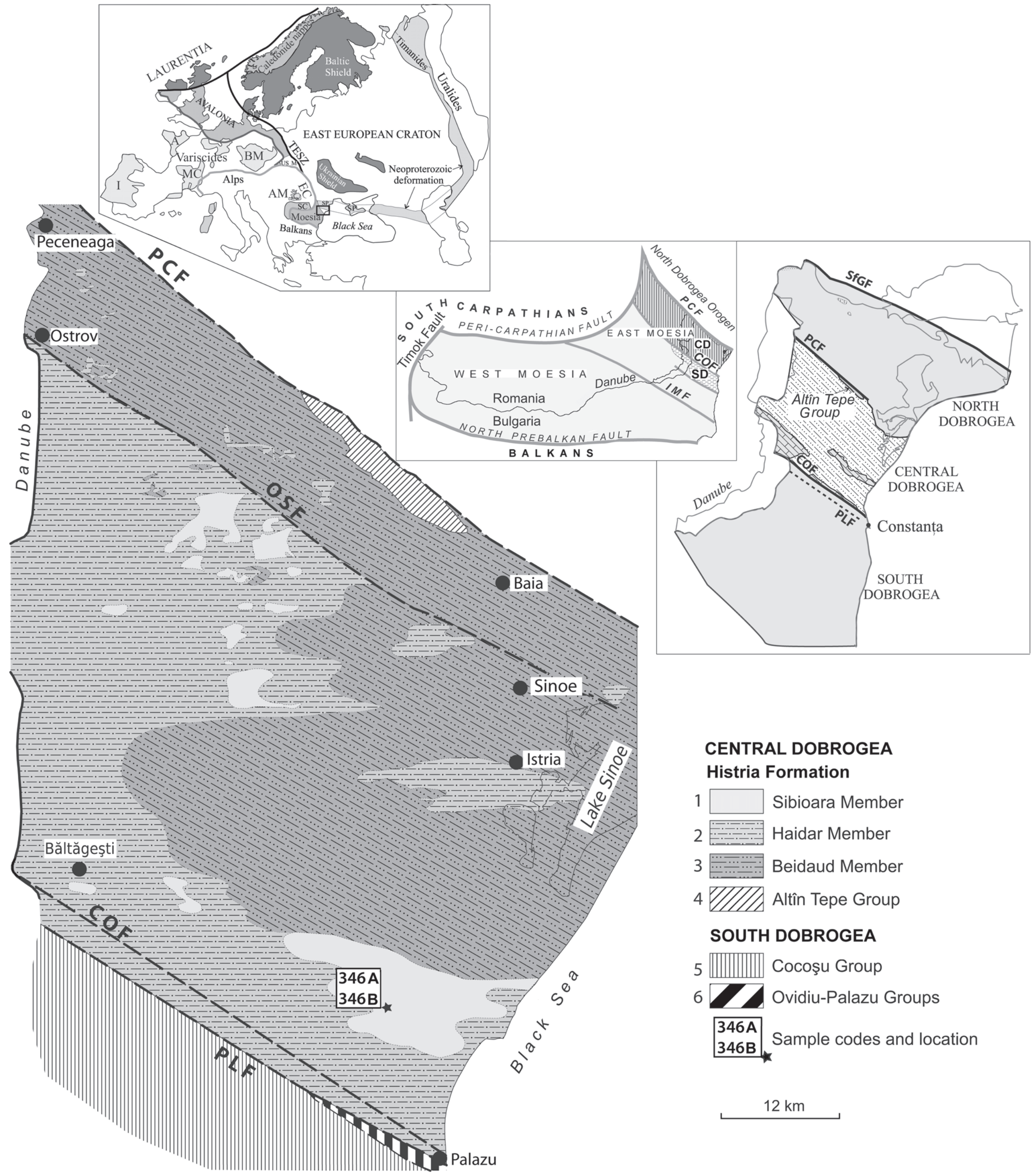

Fig. 1. Geological map of Central Dobrogea (drawn after Kräutner et al. 1988). Star mark indicates the sampling location (see text for GPS coordinates). *Topmost inset*: Location of Dobrogea area (square mark) on a map showing the basement structure and the Neoproterozoic, Caledonian, Variscan and Alpine deformation belts in Europe. **TESZ** — Trans European Suture Zone; **SC** — South Carpathians; **EC** — East Carpathians; **AM** — Apuseni Mountains; **M** — Małopolska; **US** — Upper Silesia; **SP** — Scythian Platform. Armorican Terrane Assemblage: **A** — Armorica; **MC** — Massif Central; **I** — Iberia; **BM** — Bohemian Massif. Drawn after Seghedi et al. (2005), modified. *Upper center inset*: general simplified structure of Moesia. **CD** — Central Dobrogea; **SD** — South Dobrogea; **PCF** — Peceneaga-Camena Fault; **OSF** — Ostrov-Sinoe Fault; **COF** — Capidava-Ovidiu Fault; **IMF** — Intra-Moesian Fault. Drawn after Seghedi et al. (2005), simplified. *Upper right inset*: general simplified structure of Dobrogea. **SfGF** — Sfântu Gheorghe Fault; **PCF** — Peceneaga-Camena Fault; **COF** — Capidava-Ovidiu Fault; **PLF** — Palazu Fault. Drawn after Seghedi et al. (2005), simplified.

The South Carpathian-Balkan Alpine chain surrounds Moesia to the north, west and south. The eastern Moesian margin is covered by the Black Sea and to the northeast the Early Cretaceous Peceneaga-Camena dextral transform fault (Balintoni & Baier 1997) forms the boundary with the North Dobrogea Cimmerian orogen. Moesia played a prominent role in forming the Carpathian-Balkan oroclines (e.g. Ratschbacher at al. 1993) and it is overthrusted by the Carpathian and Balkan tectonic units (e.g. Săndulescu 1984). According to Seghedi et al. (2005), West Moesia is separated from East Moesia through the Intra-Moesian Fault (Fig. 1, upper center inset). Capidava-Ovidiu Fault delimits at the surface Central Dobrogea from South Dobrogea, as components of East Moesia (Fig. 1). Oczlon et al. (2007) view West Moesia, Central Dobrogea and South Dobrogea as separate pre-Alpine terrane fragments. The authors also delineate the small Palazu terrane between Central and South Dobrogea. Regarding the basement (Fig. 2), the boundary between Central Dobrogea and South Dobrogea is the Palazu Thrust (Seghedi et al. 2005: fig. 7B). A thick cover of Paleozoic, Mesozoic, Paleocene–Eocene, Miocene, Pliocene and Quaternary sedimentary deposits overlies the greatest part of the Moesia basement. In many areas the Moesian platform sedimentary cover starts with siliciclastic sediments ascribed to the Ordovician and to some parts of the Cambrian. Four main sedimentary cycles separated by intervals of uplift and erosion have been described in the Moesian platform cover, with some differences between East and West Moesia for the Mesozoic and Cenozoic (Paraschiv 1979; Ionesi 1994). The Cambrian–Westphalian and Permian–Triassic cycles are common for the whole platform cover. The following two cycles are late Liassic–Campanian and Late Badenian–Pleistocene for West Moesia, and Late Bathonian–Early Maastrichtian and Late Badenian–Romanian for East Moesia. The basement of Moesia differs between the four components. In South Dobrogea gneisses of possible Archean age underlie a Paleoproterozoic Banded Iron Formation (BIF) and a Neoproterozoic volcano-sedimentary suite (Cocoşu Group) (Giuşcă et al. 1967; Kräutner et al. 1988). In West Moesia, several boreholes bottomed in granites and metabasites. For most metamorphic suites the Precambrian evolution is still poorly documented, and no protolith ages are available. The Central Dobrogea basement is discussed further.

Central Dobrogea

In Central Dobrogea the basement is largely exposed (Fig. 1) and consists of Neoproterozoic medium-grade metamorphic rocks (Altîn-Tepe Metamorphic Unit) and a thick late Neoproterozoic–early Cambrian turbidite succession (Histria Formation, Seghedi & Oaie 1995). The Altîn-Tepe Metamorphic Unit crops out south of the Peceneaga-Camena fault in the core of an antiformal NW trending and SE plunging fold beneath the Histria Formation. It consists of polymetamorphic rocks, with staurolite characterizing the first thermotectonic event. Biotite from micaschists yielded K/Ar ages ranging from 696 to 643 Ma (Giuşcă et al. 1967) and hornblende from amphibolites yielded 526 Ma (Codarcea-Dessila et al. 1966) (all ages recalculated by Kräutner et al. 1988). These data are interpreted either as the age of the amphibolite facies metamorphism (Giuşcă et al. 1967), or due to the partial Ar loss during the Cadomian metamorphism of the Histria Formation (Kräutner et al. 1988). The Altîn-Tepe Metamorphic Unit was traditionally regarded as the basement of the overlying Histria Formation (Ianovici & Giuşcă 1961; Giuşcă et al. 1967). The top of the metamorphic unit shows a low-grade mylonitic zone along the contact with the Histria Formation (Mureşan 1971, 1972; Kräutner et al. 1988; Seghedi & Oaie 1994). This contact was interpreted as a tectonic window below the nappe of the Histria Formation by Mureşan (1971) or as a shallow extensional detachment, as expressed by typical metamorphic core complexes (Seghedi et al. 1999). The Histria Formation is exposed over the entire area of the Central Dobrogea Shield, overlain by some remnants of an eroded Late Jurassic carbonate platform succession. West of the Danube, as proved by boreholes, Ordovician quartzitic sandstones and green shales overstep the Histria Formation. The Ordovician age is established based on graptolite records (Murgeanu & Spassov 1968). The Histria Formation consists of a turbiditic succession about 5000 m thick, representing submarine fan deposits, prograded northward in a deep basin floored by continental crust (Seghedi & Oaie 1995; Oaie 1999). Based on sedimentological data, a foreland basin setting is supposed for the Histria Formation by the cited authors. It includes a lower and an upper member dominated by sandstones and a median member consisting of distal, fine-grained turbidites. The age of the Histria Formation was ascribed to the late Neoproterozoic–Early Cambrian based on palynological assemblages

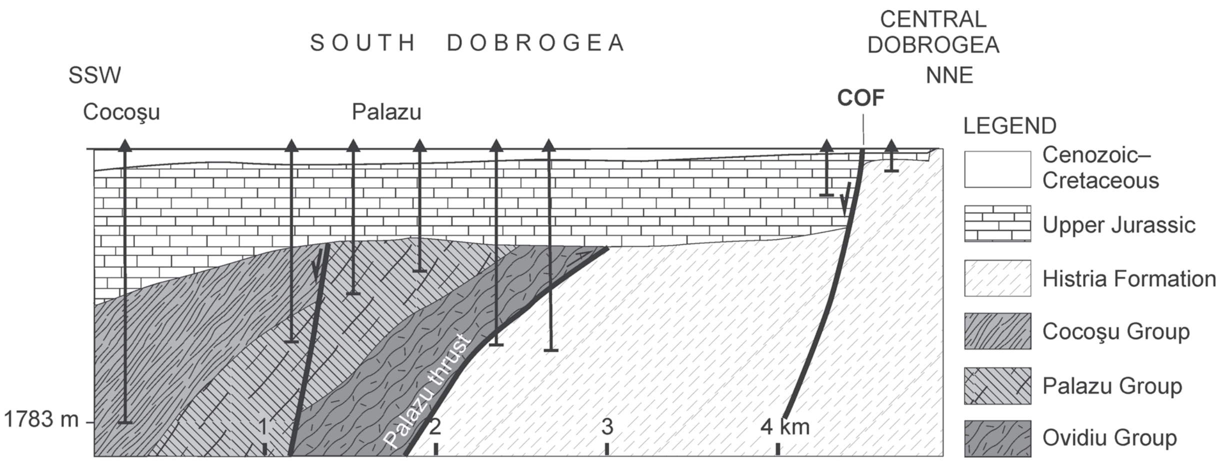

Fig. 2. Cross-section through the southernmost part of Central Dobrogea and northern part of South Dobrogea (A–B line on Fig. 1), showing the relationship between their basement rocks. Modified after Seghedi et al. (2005).

(Iliescu & Mutihac 1965) and on the medusoid record (i.e. *Nemiana simplex* Palij), identified in fine-grained turbidites (Oaie 1992, 1999). The deformation of the turbidites expressed as open folds in very low-grade metamorphic conditions took place at the end of Neoproterozoic according to K/Ar data (Giuşcă et al. 1967; Kräutner et al. 1988). Mineralogical studies indicate that the source of the turbidites was an active continental margin and its volcanic arc (Seghedi & Oaie 1995; Oaie 1999; Oaie et al. 2005). Several detrital zircons (Żelaźniewicz et al. 2001) yielded U/Pb SHRIMP ages of 1497±8 Ma, 1050±1 Ma, 603±5 Ma and 579±7 Ma, interpreted as Avalonia-type sources by Seghedi et al. (2005) or Far East Avalonia by Oczlon et al. (2007). The detrital zircon ages published by Żelaźniewicz et al. (2009) do not support their inference that Central Dobrogea could be of Baltican affinity. This is quite clear in their figure 11, where the Baltican margin has a single age projected for the entire Neoproterozoic.

Samples and method

Samples 346A and 346B (of coordinates N 44°21′28.0″/E 0.28°34′22.8″) were picked up 3 meters stratigraphically apart, from a quarry next to the Black Sea shore, on the southern shore of Lake Taşaul (Fig. 1). The samples are a very hard coarse-grained arkosian sandstone and a conglomerate, both grey to greenish in colour, with quartz, feldspar, chlorite, epidote, muscovite, a little calcite and opaque minerals in matrix. Polymictic elements consist of lithic fragments formed of the same minerals and quartz pebbles. The chlorite is a newly formed mineral and the lithic fragments are derived from acid volcanics and orthogneiss sources. In the quarry, a depositional bedding is visible, but no schistosity. Two samples with different granullometries from distinct stratigraphic levels were collected for checking the possible differences between the age distribution patterns.

For zircon extraction up to 10 kg of fresh material was sampled from each outcrop. In order to extract the zircon grains, the material has been subjected to the classical crushing, milling, gravitational separation and heavy liquids treatment. At least 100 detrital crystals were randomly selected out of each sample using a stereomicroscope and then mounted in 25 mm epoxy and polished.

The LA-ICP-MS measurements were performed at the LaserChron facility, Department of Geosciences, University of Arizona using an ISOPROBE MC-ICP-MS equipped with a New Wave DUV193 nm Excimer laser-probe with a spot diameter of 35 μm. Each grain analysis consisted of a single 20-second integration on isotope peaks without laser-firing to obtain on-peak background levels, 20 one-second integrations with the laser firing, followed finally by a 30-second purge with no laser firing in order to deliver out the remaining sample (e.g. Dickinson & Gehrels 2003). Hg contributions to ^{204}Pb were removed by taking on-peak backgrounds.

The ablated material was carried via argon gas into the IsoProbe, equipped with a sufficiently wide flight tube allowing for U and Pb isotopes to be measured simultaneously. Measurements were done in static mode, using Faraday detectors for ^{238}U, ^{232}Th, $^{208-206}$Pb, and an ion-counting channel for ^{204}Pb.

Common Pb corrections were made using the measured ^{204}Pb and assuming initial Pb compositions from Stacey & Kramers (1975). Analyses of zircon standards of known isotopic and U-Pb composition were conducted in most cases after each set of five unknown measurements to correct for elemental isotopic fractionation.

The samples were analysed in hard extraction mode, which yielded higher and more variable Pb/U fractionation. The ^{206}Pb*/^{238}U values for the standards were corrected for an average of 15.3 % (±2.6 %) and 27.2 % (±3.0 %) fractionation (uncertainties at 2σ standard deviation of ~20 analyses), respectively. The U/Pb measurements, ratios, ages and errors are shown in the Supplementary data Table (available in the electronic edition at www.geologicacarpathica.sk). Using the ISOPLOT program of Ludwig (2001), Concordia diagrams (with data point error symbols at 1σ) for each sample were plotted. The ^{206}Pb/^{238}U ages are considered best if younger than 800 Ma and ^{207}Pb/^{206}Pb ages if older than 800 Ma (e.g. Gehrels et al. 2008 and references therein), and further plotted on binary age vs. number of ages distribution diagrams. Analyses that have greater than 10 % uncertainty, are more than 30 % discordant or 5 % reverse discordant, are excluded from further consideration.

Results

Sample 346A

Some of the zircon grains are well rounded ball-like or barrel-like in form, colourless or sometimes red in nuance, completely transparent. These grains suffered a long transport. Other grains represent prisms or prism fragments of different sizes, broken during the processing of samples, not very well abraded, transparent, colourless or slighty yellowish in colour, sometimes reddish. Their forms suggest a relatively short transport. The ages of 84 dated zircon grains range between 594 Ma and 3307 Ma, that is between the late Neoproterozoic (Ediacaran) and late Paleoarchean (Supplementary data Table at www.geologicacarpathica.sk). We point out the important Archean source. Significant peaks indicating the orogenic sources are visible between 0.55–0.75 Ga (Neoproterozoic), 1.25–1.4 Ga and 1.45–1.7 Ga (Mesoproterozoic to the latest Paleoproterozoic), 1.95–2.2 Ga (Paleoproterozoic) and between 2.7–3.0 Ga (Neoarchean to Mesoarchean). There are also several Paleoarchean ages. Age gaps or low density intervals appear between 0.75–1.25 Ga, around 1.8 Ga and between 2.2–2.7 Ga. Similar to the age peaks, the age gaps have their significance from the point of view of sources.

Sample 346B

Zircon grains from this sample are similar to those from sample 346A, but are a little bigger. The ages of 96 dated zircon grains range between 583 Ma and 3135 Ma (Supplementary data Table available at www.geologicacarpathica.sk). The age distribution has similar patterns in the two samples (Fig. 3a,b,d). It is only the number of ages in the corresponding clusters that produce low or high peaks. In this sample the concentration of Archean ages is higher, with ages in the 1.0–1.25 Ga interval (Grenvillian orogeny). As the two diagrams show similar distribution patterns, it seems reasonable to combine them in a single diagram (Fig. 3c). The orogenic sources of the detrital zircon are discussed later. We signalize here the low U/Th ratio in the dated zircons (Supplementary data Table at www.geologicacarpathica.sk) characteristic to magmatic zircon. The arrangement of ages around Concordia (Fig. 4) indicates high concordance between $^{238}U/^{206}Pb$ and $^{235}U/^{207}Pb$ ages. This is a general feature of detrital zircon, due to natural selection during weathering, transport and sedimentary processes.

Discussion

The age of the Histria Formation

The two samples yielded ten Ediacaran ages (5.5 % from all the ages) ranging between 633 and 583 Ma. From Histria Formation rocks Żelaźniewicz et al. (2009) also reported five Ediacaran U/Pb ages based on detrital zircon, ranging between 622 and 579 Ma. These data suggest a maximum late Ediacaran depositional age for the Histria Formation. Correlating the U/Pb detrital zircon ages with the age indicated by the medusoid *Nemiana simplex* Palij identified in fine-grained turbidites by Oaie (1992, 1999) the late Ediacaran–possibly earliest Cambrian age of the Histria Formation is firmly established.

Terrane provenance

The significance of terms

It is necessary to constrain the meaning of some terms because the notions evolved through time. A recent classification of peri-Gondwanan terranes (Nance et al. 2008) discerns between the (1) Avalonian, (2) Cadomian, (3) Ganderian and (4) Cratonic type.

The *Avalonian* terranes originated as oceanic volcanic arcs within the Panthalassa Ocean surrounding Rodinia. These terranes accreted to the Gondwana margin by ca. 650 Ma. The Panthalassic island arcs were also called Proto-Avalonian terranes by Nance et al. (2002). Regarding their detrital zircon, the *Avalonian* terranes were derived dominantly from the Amazonian craton. The *Ganderian* and *Cratonic* terranes also represent peri-Amazonian terranes by their detrital zircon sources, formed either of recycled crust (Ganderian terranes) or of material unaffected by the Avalonian-Cadomian continental margin magmatism (Cratonic terranes). The *Cadomian* terranes were provideded with detrital zircon from the African craton. According to Nance et al. (2008) the Avalonian terranes

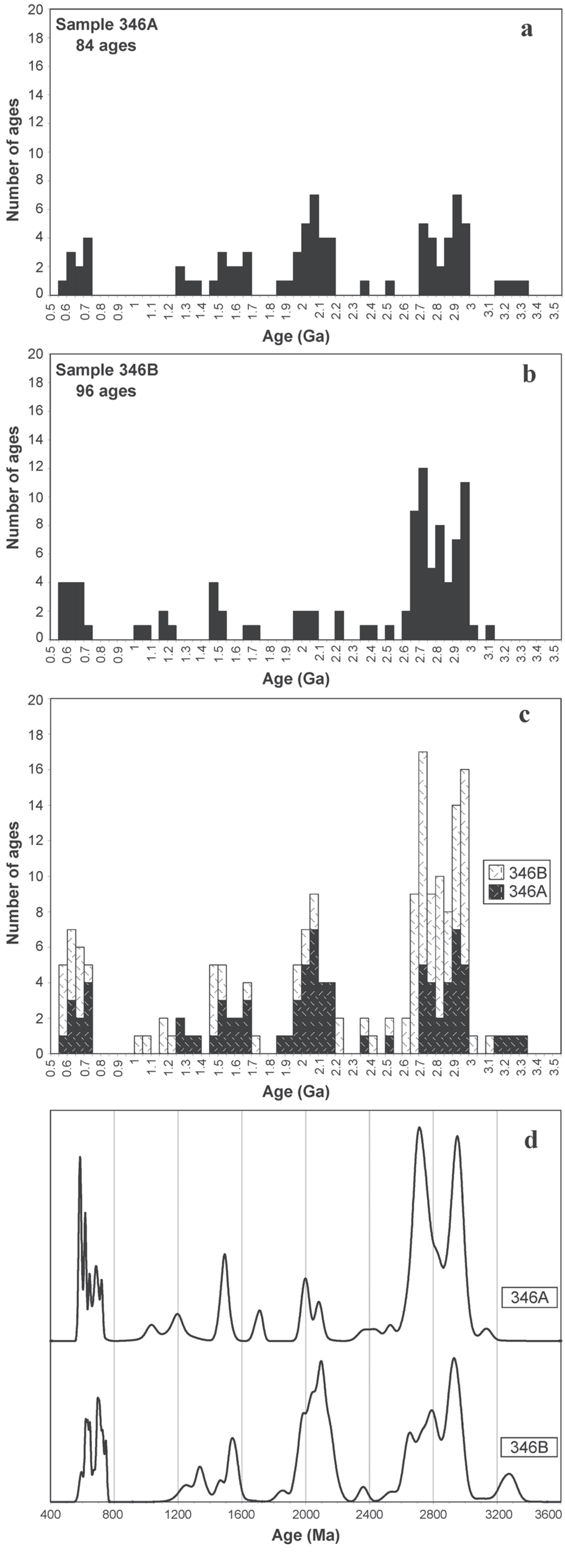

Fig. 3. U-Pb ages distribution of sample 346A (**a**) and 346B (**b**) and overall distribution of both samples (**c**) without considering 1σ absolute errors. Stacked normalized probability plot of both samples (**d**) is figured for a better comparison of age distribution spectra.

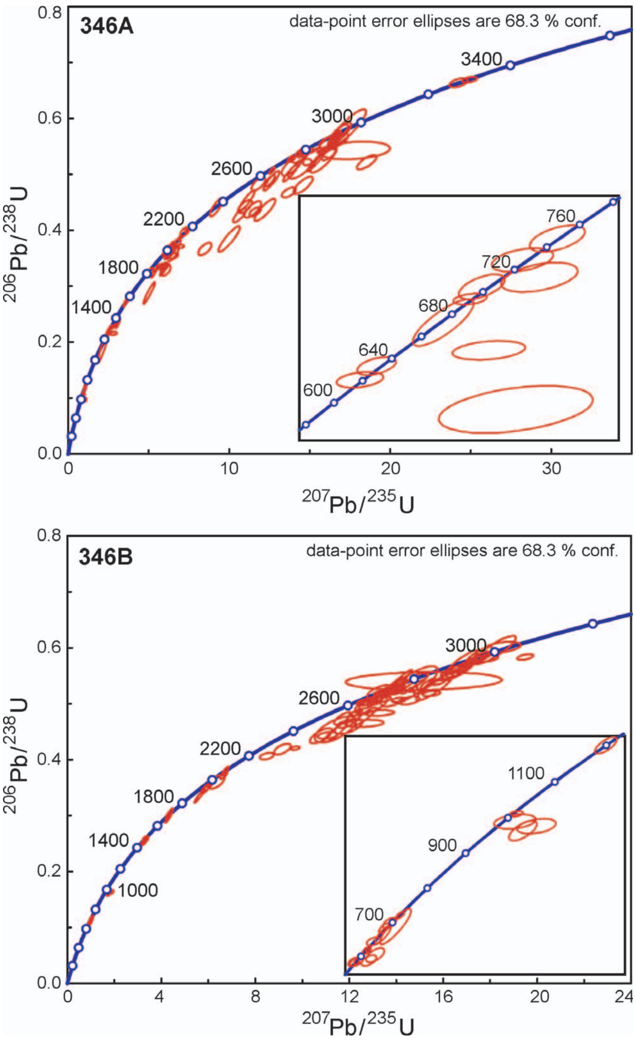

Fig. 4. Concordia projection of detrital ages for samples 346A and 346B.

rifted off from the Gondwana margin beginning in the Early Ordovician. However, Winchester et al. (2002) and Żelaźniewicz et al. (2009) advocate a peri-Amazonian provenance but a pre-Ordovician (Cambrian) drifting for some terranes adjacent to TESZ. In summary, the peri-Amazonian terranes can be of Avalonian, Ganderian or Cratonic type, some of them leaving Gondwana margin during the Cambrian Period and others during the Ordovician Period. In order to distinguish between them we should say Cambrian-Avalonian, Cambrian-Ganderian, or Cambrian-Cratonic type terranes and Ordovician-Avalonian, Ordovician-Ganderian or Ordovician-Cratonic type terranes.

Previous provenance hypotheses

In the following, the terms are those used by the cited authors with or without distinction between the Moesia composite terrane and Moesian platform. Up to now the origin of the Central Dobrogea has been discussed only in a very general manner. According to Pharaoh (1999), "The affinity of the terrane(s) underlying the Moesian Platform is poorly constrained at present". According to Winchester et al. (2002), Central Dobrogea, Southern Dobrogea and the Moesian platform have a common origin with the Bruno-Silesia, Łysogóry and Małopolska terranes. Six hundred and fifty Ma ago they were in contiguity with Amazonia and Baltica as components of the supercontinent Pannotia and left Amazonia between 550–520 Ma. Von Raumer et al. (2002) attached the Istanbul, Moesia and Zonguldak terranes to Baltica before 490 Ma. Stampfli et al. (2002) consider these terranes as Avalonia. Von Raumer et al. (2003) view the Istanbul and Moesia terranes as Avalonian satellites and attach the Zonguldak terrane to Baltica. Winchester et al. (2006) attribute to Central Dobrogea a peri-Baltican affinity, together with Bruno-Silesia, Łysogóry and Małopolska. As we already mentioned, Seghedi et al. (2005) and Oczlon et al. (2007) supposed an Avalonian provenance for Central Dobrogea based on some Rondonian and Grenvillian detrital zircon ages obtained by Żelaźniewicz et al. (2001). Żelaźniewicz et al. (2009) view the Central (and South) Dobrogea as having Baltican provenance inspite of the presence of Neoproterozoic detrital zircon suppliers in Central Dobrogea and the absence of these sources in Baltica, according to their own data. Kalvoda & Bábek (2010) incorporate the Brunovistulia, Małopolska and West Moesia terranes into the late Neoproterozoic–Cambrian Baltican margin. Regarding the Istanbul-Zonguldak, Bittesh and East Moesia terranes, these authors say that they "may have been part of the Avalonian terrane assemblage, although an Arabian-Nubian Shield or Baltican provenance cannot be excluded". Such contradictory hypotheses reflect the insuffcicency of the data and an illustration of them can be found in Balintoni et al. (2010a).

Provenance of Central Dobrogea

The main features of our diagrams can be summarized as follows: i) an important age group is situated in the late Neoproterozoic; ii) there is an age spreading along the Mesoproterozoic with a peak around 1.5 Ga; iii) the Paleoproterozoic contains age concentrations around 1.7 Ga and between 1.95–2.2 Ga; iv) the greatest age grouping is Archean, between 2.65–3.0 Ga; v) a very low frequency of data appears around 1.8 Ga and between 2.2–2.6 Ga.

Comparing our data with the data from the Arabian-Nubian Shield (Johnson & Woldehaimanot 2003) and from Iran (Horton et al. 2008) we notice the absence of the Mesoproterozoic zircons in these regions, except the Grenvillian sources.

Considering the data presented by Samson et al. (2005), Linnemann et al. (2007), Rino et al. (2008) and Bogdanova et al. (2008), suppliers for the Mesoproterozoic detrital zircon in the terranes amalgamated between Gondwana and Laurussia or docked to Laurussia during the Paleozoic could be Baltica, Laurentia and Amazonia. Due to a magmatic quiescence period in Laurentia between 1.61 and 1.49 Ga (e.g. Samson et al. 2005) and the absence of the late Neoproterozoic Cadomian events (e.g. Linnemann et al. 2007), this continent can be excluded as the original place of the Central Dobrogea terrane.

Discrimination between Baltica and Amazonia as the motherland of the Central Dobrogea terrane can be done based on the Neoproterozoic suppliers, because according to

Kuznetsov et al. (2010), the zircons with ages between 0.75 and 0.6 Ga are missing in Baltica. The data of Żelaźniewicz et al. (2009) are in accordance with this point of view, because they recorded a single detrital zircon age of 841 Ma in the Ediacaran cover of the East European Craton margin. This age span being well represented in the Central Dobrogea terrane, we conclude that it was a part of the Gondwanan Amazonian margin, that is, it has a peri-Amazonian origin. Whether the Central Dobrogea is of Cambrian-Avalonian or -Ganderian type terrane depends on the Altîn Tepe sequence U/Pb and Sm/Nd ages, unsolved until now.

Orogenic sources of the detrital zircons

For the Central Dobrogea terrane the Brasiliano orgen (e.g. Nance et al. 2009) is the most important Neoproterozoic detrital zircon source. Regarding the Mesoproterozoic, Paleoproterozoic and Archean sources, they are quite similar to the present-day sources of detrital zircon described by Rino et al. (2008) at the Amazon and Niger rivers mouths (i.e. group 2 of zircon population), which confirm the peri-Amazonian provenance of the Central Dobrogea. It is characteristic to the Amazon River detrital zircons that they occur along the entire 1.0–2.0 Ga interval but at a low frequency and the very important peaks between 2.0–2.2 Ga and older than 2.5 Ga. A good coverage around 3.0 Ga, as visible in our diagrams is found in the Parana River detrital zircons, classified in Group 3 of zircon populations by Rino et al. (2008). If we consider the granitoid events in space and time (Condie et al. 2009), then again the age pattern of the South America detrital zircon is the closest to the Central Dobrogea pattern. Consequently, the Mesoproterozoic and Paleoproterozoic accretionary orogens as well as the Archean nuclei (e.g. Carajas) of the Amazonian craton (e.g. Cordani & Texeira 2007) provided the detrital zircon within the Cadomian forearc basin of the Central Dobrogea. The relatively slight contribution of the Grenvillian sources and the remarkable input from Paleoproterozoic and Archean sources, suggest an initial location of the Central Dobrogea not far from the West African Craton. The Amazonian sources illustrated by Nance et al. (2009) including the relative gaps around 1.8 Ga and between 2.2–2.6 Ga almost perfectly correlate with the Central Dobrogea sources. Consequently, the Central Dobrogea terrane represents a peri-Amazonian crustal fragment that joined other Moesia basement components during the Cambrian Period.

Correlations

Argumented correlations can be only based on the data reported by Żelaźniewicz et al. (2009). Central Dobrogea shows a similar pattern of the detrital zircon ages with those from Brunovistulia and West Małopolska. Brunovistulia is viewed by Żelaźniewicz et al. (2009) as a peri-Amazonian composite terrane, which migrated toward Baltica during the Cambrian. Małopolska is considered a peri-Baltican terrane, but strictly the detrital zircon ages contradict this inference. As discussed, the Central Dobrogea attached to NE Moesia before the Ordovician, knowing that sediments of this age cover the Palazu fault. As a conclusion, Central Dobrogea correlates with Brunovistulia and probably Małopolska from the provenance and migration time perspectives.

Conclusions

The Central Dobrogea terrane is constituted of the Altîn Tepe basement of unknown age and its cover, the flysch-like Histria Formation. A metasandstone and a metaconglomerate sample from the Histria Formation furnished detrital zircon. A group of ten early Ediacaran ages yielded by the

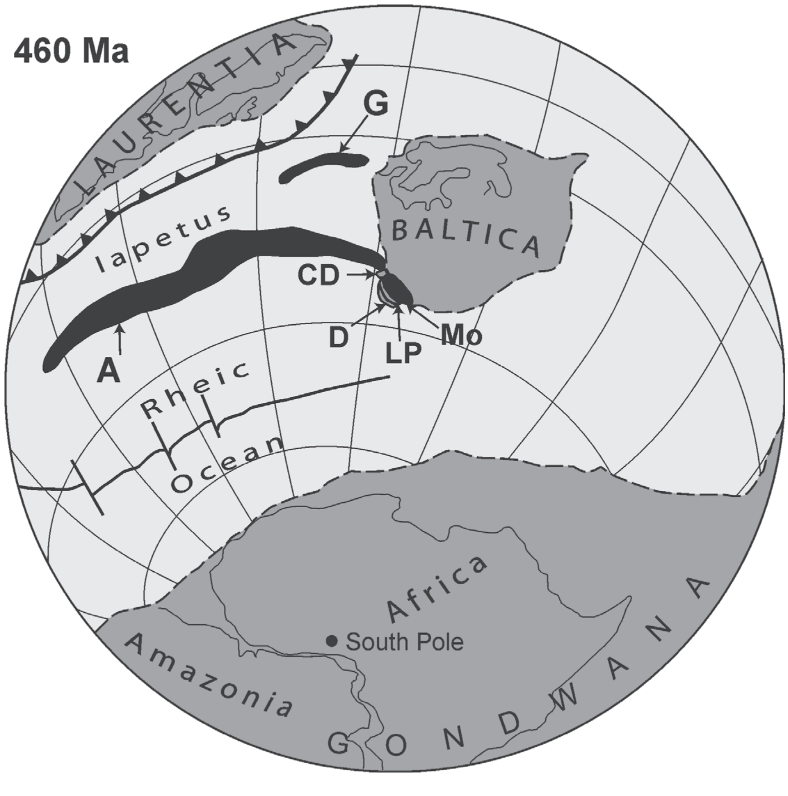

Fig. 5. Paleogeographic configuration at 460 Ma of the peri-Amazonian terranes in accordance with the data and hypotheses discussed in the text. Paleocontinents configuration drawn according to Nance et al. (2010). The peri-Amazonian terranes context is simplified and modified according to Balintoni et al. (2010: fig. 9d). The stages in the history of the peri-Amazonian terranes are presented in that figure. Peri-Amazonian terranes: **A** — Ordovician-Avalonia; **D** — Drăgșan; **LP** — Lainici-Păiuș; **Mo** — Moesia; **CD** — Central Dobrogea; **G** — Ordovician-Ganderia. Moesia drifted to Baltica before 500 Ma. Post 500 Ma the Ordovician-Ganderia migrated toward Baltica in front of the Ordovician-Avalonia, and a fragment of the first terrane attached to Moesia (Lainici-Păiuș terrane). Behind Avalonia drifted the Drăgșan terrane, that attached to Lainici-Păiuș terrane.

detrital zircon establish as late Ediacaran the maximum possible deposition age of the Histria Formation. The age distribution pattern coincides with those of the peri-Amazonian terranes that received material from the Amazon craton orogens, that is the Central Dobrogea has a peri-Amazonian provenance. Drill-holes in the Moesian platform cover met Ordovician sediments overlying the Palazu reverse fault, the boundary between Central Dobrogea and South Dobrogea. This situation suggests a Cambrian junction between Central Dobrogea and the other components of Moesia forming the Moesia composite terrane that migrated toward Baltica during the Cambrian Period, too (Fig. 5). Central Dobrogea can be correlated with the Brunovistulia and probably Małopolska terranes from Central Europe from the provenance and drifting time perspective. Implicitly we suppose a Gondwanan origin of the whole of Moesia, because a peri-Amazonian terrane became attached to its NE margin during the Cambrian and toward the west and south Ordovician-Avalonian terranes docked to it (Balintoni et al. 2010).

Acknowledgments: This research was financially supported by Grant ID-480 CNCSIS. The authors wish to express their gratitude to Jiří Kalvoda and especially to Niko Froitzheim, for their careful revisions and insightful suggestions and observations, which improved the quality of this paper. V. Valencia is gratefully acknowledged for his help with analytical procedures and for his careful supervision of data acquisition.

References

Balintoni I. 1997: Geotectonics of Romanian metamorphic terranes. *Ed. Carpatica*, Cluj Napoca (in Romanian).

Balintoni I. & Baier U. 1997: Theoretical constrains on the relationship between the Alpine structures of North Dobrogea and the Peceneaga — Camena fault. *Studia Univ. Babeş-Bolyai, Geologia* XLII, 2, 52–66.

Balintoni I., Balica C., Ducea M. & Stremtan C. 2010: Peri-Amazonian, Avalonian-type and Ganderian-type terranes in the South Carpathians, Romania: The Danubian domain basement. *Gondwana Res*. doi: 10.1016/j.gr.2010.10.002

Balintoni I., Balica C., Seghedi A. & Ducea M.N. 2010a: Avalonian and Cadomian terranes in North Dobrogea, Romania. *Precambrian Res.* doi: 10.1016/j.precamres.2010.08.010

Bogdanova S.V., Bingen B., Gorbatschev R., Kheraskova T.N., Kozlov V.I., Puchkov V.N. & Volozh Y.A. 2008: The East European Craton (Baltica) before and during the assembly of Rodinia. *Precambrian Res.* 160, 23–45.

Codarcea-Dessila M., Mirăuţă O., Semenenko N.P., Demidenko S.G. & Zeidis B. 1966: Geological interpretation of data obtained through K-Ar method on the absolute age of metamorphic formations from Southern Carpathians and Dobrogea. *Tr XII sess. Kono opredelenia absoliutnovo vozrasta gheologhiceskih formacii pri NZANDDr*, Moskva, 5–16 (in Russian).

Condie K.C., Belousova E.A., Griffin W.L. & Sircombe K.N. 2009: Granitoid events in space and time: Constraints from igneous and detrital zircon age spectra. *Gondwana Res.* 15, 228–242.

Cordani U.G. & Teixeira W. 2007: Proterozoic accretionary belts in the Amazonian Craton. In: Hatcher R.D.J., Carlson M.P., McBride J.H. & Martinez Catalan J.R. (Eds.): 4-D framework of continental crust. *Geol. Soc. Amer. Mem.* 200, 297–320.

Dickinson W.R. & Gehrels G.E. 2003: U-Pb ages of detrital zircons from Permian and Jurassic eolian sandstones of the Colorado Plateau, USA: paleogeographic implications. *Sed. Geol.* 163, 22–66.

Fernández-Suárez J., Gutierez Alonso G. & Jeffries T.E. 2002: The importance of along-margin terrane transport in northern Gondwana: insights from detrital zircon parentage in Neoproterozoic rocks from Iberia and Brittany. *Earth Planet. Sci. Lett.* 204, 75–88.

Gehrels G.E., Valencia V. & Ruiz J. 2008: Enhanced precision, accuracy, efficiency, and spatial resolution of U-Pb ages by laser ablation-multicollector-inductively coupled plasma-mass spectrometry. *Geochem. Geophys. Geosyst.* 9, 3, Q03017, doi:10.1029/2007GC001805

Giuşcă D., Ianovici V., Mînzatu S., Soroiu E., Lemne M., Tănăsescu A. & Ioncică M. 1967: On the absolute age of the metamorphic rocks in the foreland of the Carpathian orogen. *Stud. Cerc. Geol. Geofiz. Geogr., Ser. Geol. (Bucuresti)* 12, 287–297 (in Romanian).

Golonka J. 2002: Plate-tectonics maps of the Phanerozoic. In: Kiessling W., Flugel E. & Golonka J. (Eds.): Phanerozoic reef patterns. *SEPM Spec. Publ.* 72, 21–75.

Horton B.K., Hassanzadeh J., Stockli D.F., Axen G.J., Gillis R.J., Guest B., Amini A., Fakhari M., Zamanzadeh M.S. & Grove G. 2008: Detrital zircon provenance of Neoproterozoic to Cenozoic deposits in Iran: Implications for chronostratigraphy and collisional tectonics. *Tectonophysics* 451, 97–122.

Ianovici V. & Giuşcă D. 1961: New data on the Moldavian and Dobrogea plateaus basements. *Stud. Cerc. Geol., Acad. RSR* VI, 1, 153–159 (in Romanian).

Iliescu V. & Mutihac V. 1965: Considerations on the correlation possibilities of Tulcea zone basement and Central Dobrogea folded basement. *D. S. Inst. Geol. Geofiz.* LI/1, 243–249 (in Romanian).

Ionesi L. 1994: Geology of North-Dobrogea Orogen and platform units. *Ed. Tehnică*, Bucureşti, 1–280 (in Romanian).

Johnson P.R. & Woldehaimanot B. 2003: Development of the Arabian-Nubian Shield: perspectives on accretion and deformation in the northern East African Orogen and the assembly of Gondwana. In: Yoshida M., Dasgupta S. & Windley B. (Eds.): Proterozoic East Gondwana: Supercontinent assembly and breakup. *Geol. Soc. London, Spec. Publ.* 206, 289–325.

Kalvoda J. & Bábek O. 2010: The margins of Laurussia in Central and Southeast Europe and Southwest Asia. *Gondwana Res.* 17, 2–3, 526–545.

Kräutner H.G., Mureşan M. & Seghedi A. 1988: Precambrian of Dobrogea. In: Zoubek V. (Ed.): Precambrian in younger fold belts. *John Wiley*, New York, 361–379.

Kuznetsov N.B., Natapov L.M., Belousova E.A., O'Reilley S.Y. & Griffin W.L. 2010: Geochronological, geochemical and isotopic study of detrital zircon suites from late Neoproterozoic clastic strata along the NE margin of the East European Craton: Implications for plate tectonic models. *Gondwana Res.* 17, 2–3, 583–601.

Linnemann U., McNaughton N.J., Romer R.L., Gemlich M., Drost K. & Tonk C. 2004: West African provenance for Saxo-Thuringia (Bohemian Massif): Did Armorica ever leave pre-Pangean Gondwana? — U/Pb SHRIMP zircon evidence and the Nd-isotopic record. *Int. J. Earth Sci. (Geol. Rundsch.)* 93, 5, 683–705.

Linnemann U., Gerdes A., Drost K. & Buschmann Â. 2007: The continuum between Cadomian orogenesis and opening of the Rheic Ocean: Constraints from LA-ICP-MS U-Pb zircon dating and analysis of plate-tectonic setting (Saxo-Thuringian zone, northeastern Bohemian massif, Germany). In: Linnemann U., Nance R.D., Kraft P. & Zulauf G. (Eds.): The evolution of the Rheic Ocean. *Geol. Soc. Amer., Spec. Pap.* 423, 61–96.

Ludwig K.R. 2001: Isoplot/Ex, rev. 2.49: A geochronological toolkit for Microsoft Excel. *Berkeley Geochronology Center, Spec. Publ.* No. 1a, 1–58.

Matte P., Maluski H., Rajlich P. & Franke W. 1990: Terrane boundaries in the Bohemian Massif: Result of large scale Variscan shearing. *Tectonophysics* 177, 151–170.

Mureşan M. 1971: On the presence of a tectonic window in the Green Schists area frim Central Dobrogea. *Dari Seama Inst. Geol.* LVII, 5, 127–154 (in Romanian).

Mureşan M. 1972: Studies on the pyrite ore deposit from Altîn Tepe (Central Dobrogea). II. Stratigraphic position of mineralisation. *Dari Seama Inst. Geol.* LVIII, 2, 25–61 (in Romanian).

Murgeanu G. & Spassov H. 1968: Les Graptolites du forage Bordei Verde (Roumanie). *Bulgarian Acad. Sci., Committee of Geology, Bull. Geol. Inst., Ser. Paleont. K.H.* 17, 229–239.

Nance R.D. & Murphy J.B. 1996: Basement isotopic signatures and Neoproterozoic paleogeography of Avalonian–Cadomian and related terranes in the Circum-North Atlantic. In: Nance R.D. & Thompson M.D. (Eds.): Avalonian and related peri-Gondwanan terranes of the Circum-North Atlantic. *Geol. Soc. Amer., Spec. Pap.* 304, 333–346.

Nance R.D., Murphy J.B. & Keppie J.D. 2002: Cordilleran model for the evolution of Avalonia. *Tectonophysics* 352, 11–31.

Nance R.D., Murphy J.B., Strachan R.A., Keppie J.D., Gutierez Alonso G., Fernández-Suárez J., Quesada C., Linnemann U., D'Lemos R.S. & Pisarevsky S.A. 2008: Neoproterozoic–early Palaeozoic tectonostratigraphy and palaeogeography of the peri-Gondwanan terranes: Amazonian v. West African connections. In: Ennih N. & Liegeois J.-P. (Eds.): The boundaries of the West African craton. *Geol. Soc. London*, *Spec. Publ*. 297, 345–383.

Nance R.D., Keppie J.D., Miller B.V., Murphy J.B. & Dostal J. 2009: Palaeozoic palaeogeography of Mexico: constraints from detrital zircon age data. In: Murphy J.B., Keppie J.D. & Hynes A.J. (Eds.): Ancient orogens and modern analogues. *Geol. Soc. London*, *Spec. Publ.* 327, 239–269.

Nance R.D., Gutierez Alonso G., Keppie J.D., Linnemann U., Murphy J.B., Quesada C., Strachan R.A. & Woodcock N. 2010: Evolution of the Rheic Ocean. *Gondwana Res.* 17, 2–3, 194–222.

Oaie G. 1992: Traces of organic activity in the Greenschist Series of central Dobrogea (Romania). *Stud. Cerc. Geol.* 37, 77–81.

Oaie G. 1999: *S*edimentology and tectonics of the Green Schists Series from Central Dobrogea and their prolongation in the Black Sea offshore. *Unpubl. Ph.D. Thesis*, *University of Bucharest*, 1–105 (in Romanian).

Oaie G., Seghedi A., Rădan S. & Vaida M. 2005: Sedimentology and source area composition for the Neoproterozoic-Eocambrian turbidites from East Moesia. *Geol. Belgica* 8/4, 78–105.

Oczlon M.S., Seghedi A. & Carrigan C.W. 2007: Avalonian and Baltican terranes in the Moesian Platform (southern Europe, Romania, and Bulgaria) in the context of Caledonian terranes along the southwestern margin of the East European craton. *Geol. Soc. Amer., Spec. Pap.* 423, 375–400.

Paraschiv D. 1979: Moesian platform and its hydrocarbon reservoirs. *Ed. Academiei*, Bucureşti, 1–195 (in Romanian).

Pharaoh T.C. 1999: Palaeozoic Terranes and their lithospheric boundaries within the Trans-European Suture Zone, TESZ, a review. *Tectonophysics* 314, 17–41.

Rino S., Kon Y., Sato W., Maruyama S., Santosh M. & Zhao D. 2008: The Grenvillian and Pan-African orogens: World's largest orogenies through geologic time, and their implications on the origin of superplume. *Gondwana Res.* 14, 51–72.

Samson S.D., D'Lemos R.S., Miller B.V. & Hamilton M.A. 2005: Neoproterozoic paleogeography of the Cadomia and Avalon terranes: constraints from detrital zircons. *J. Geol. Soc. London* 162, 65–71.

Săndulescu M. 1984: Geotectonica României. *Ed. Tehnică*, Bucureşti, 1–336.

Seghedi A. & Oaie G. 1994: Tectonic setting of two contrasting types of pre-Alpine basement: North versus Central Dobrogea. *Abstracts Volume, ALCAPA II Conference, Rom. J. Tect. Reg. Geol.* 75, Suppl. 1, 56.

Seghedi A. & Oaie G. 1995: Palaeozoic evolution of North Dobrogea. In: Săndulescu M., Seghedi A., Oaie G., Grădinaru E. & Rădan S. (Eds.): Field Guidebook, Central and North Dobrogea. *IGCP Project No. 369 "Comparative evolution of Peri-Tethyan Rift Basins"*, Mamaia 1995, 1–75.

Seghedi A., Berza T., Iancu V., Mărunţiu M. & Oaie G. 2005: Neoproterozoic terranes in the Moesian Basement and in the Alpine Danubian Nappes of the South Carpathians. *Geol. Belgica* 8, 4, 4–19.

Seghedi A., Oaie G., Iordan M., Avram E., Tatu M., Ciulavu D., Vaida M., Rădan S., Nicolae I., Seghedi I., Szákacs A. & Drăgănescu A. 1999: Excursion Guide of the Joint Meeting of EUROPROBE TESZ, PANCARDI and GEORIFT Projects: "Dobrogea — the interface between the Carpathians and the Trans-European Suture Zone": Geology and structure of the Precambrian and Paleozoic basement of North and Central Dobrogea. Mesozoic history of North and Central Dobrogea. *Rom. J. Tect. Reg. Geol.* 77, Suppl. 2, 1–72.

Stacey J.S. & Kramers J.D. 1975: Approximation of terestrial lead isotope evolution by a two stage model. *Earth Planet. Sci. Lett.* 26, 207–221.

Stampfli G.M., von Raumer J.F. & Borel G.D. 2002: Paleozoic evolution of pre-Variscan terranes; from Gondwana to the Variscan collision. In: Martinez Catalan J.R., Hatcher R.D., Arenas R. & Diaz Garcia F. (Eds.): Variscan-Appalachian dynamics: The building of the late Paleozoic basement. *Geol. Soc. Amer., Spec. Pap.* 364, 263–280.

von Raumer J.F., Stampfli G.M., Borel G. & Bussy F. 2002: Organization of pre-Variscan basement areas at the North-Gondwanan margin. *Int. J. Earth Sci. (Geol. Rundsch.)* 91, 1, 35–52.

von Raumer J.F., Stampfli G.M. & Bussy F. 2003: Gondwana-derived microcontinents — the constituents of the Variscan and Alpine collisional orogens. *Tectonophysics* 365, 7–22.

Winchester J.A. & The PACE TMR Network Team, contract ERBFMRXCT97-0136, 2002: Palaeozoic amalgamation of Central Europe: new results from recent geological and geophysical investigations. *Tectonophysics* 360, 5–21.

Winchester J.A., Pharaoh T.C., Verniers J., Ioane D. & Seghedi A. Palaeozoic accretion of Gondwana-derived terranes to the East European Craton: recognition of detached terrane fragments dispersed after collision with promontories. In: Gee D.G. & Stephenson R.A. (Eds.): European lithosphere dynamics. *Geol. Soc. Mem.* 32, 323–332.

Yanev S., Lakova I., Boncheva I. & Sachanski V. 2005: The Moesian and Balkan Terranes in Bulgaria: Palaeozoic Basin Development, palaeogeography and tectonic evolution. *Geol. Belgica* 8, 4, 185–192.

Ziegler P. 1986: Geodynamic model for the Paleozoic crustal consolidation of W and C Europe. *Tectonophysics* 126, 303–328.

Żelaźniewicz A., Seghedi A., Jachowicz M., Bobiński W., Buła Z. & Cwojdzinski S. 2001: U-Pb SHRIMP data confirm the presence of a Vendian foreland flysch basin next to the East European Craton. *Abstr.*, *EUROPROBE Conference,* Ankara, Turkey, 98–101.

Żelaźniewicz A., Buła Z., Fanning M., Seghedi A. & Żaba J. 2009: More evidence on Neoproterozoic terranes in Southern Poland and southeastern Romania. *Geol. Quart.* 53, 1, 93–124.

Zulauf G., Romano S.S., Doerr V. & Fiala J. 2007: Crete and Minoan terranes: Age constraints from U-Pb dating of detrital zircons. In: Linnemann U., Nance R.D., Kraft P. & Zulauf G. (Eds.): The evolution of the Rheic Ocean: From Avalonian–Cadomian active margin to Alleghenian–Variscan Collision. *Geol. Soc. Amer., Spec. Pap.* 423, 401–411.

Supplementary data Table: Analytical data for samples 346A and 346B. *Commentary on the table see at the end.*

Analysis	Isotope ratios										Apparent ages (Ma)								
	U (ppm)	206Pb 204Pb	U/Th	206Pb* 207Pb*	± (%)	207Pb* 235U*	± (%)	206Pb* 238U	± (%)	error corr.	206Pb* 238U*	± (Ma)	207Pb* 235U	± (Ma)	206Pb* 207Pb*	± (Ma)	Best age (Ma)	± (Ma)	Conc (%)
RO346A-3	565	16524	2.2	12.1657	2.0	2.3800	4.0	0.2100	3.5	0.87	1228.8	38.8	1236.6	28.7	1250.3	39.4	1250.3	39.4	98.3
RO346A-4	368	29628	5.6	7.9464	3.8	5.8179	3.8	0.3353	0.5	0.13	1864.0	8.1	1949.1	33.1	2040.7	66.9	2040.7	66.9	91.3
RO346A-5	322	4416	1.3	7.4307	2.5	6.0796	3.0	0.3276	1.8	0.59	1826.9	28.5	1987.3	26.5	2158.5	42.8	2158.5	42.8	84.6
RO346A-6	400	26212	5.5	7.7986	3.5	5.9753	3.5	0.3380	0.5	0.14	1876.9	8.1	1972.3	30.9	2073.8	61.9	2073.8	61.9	90.5
RO346A-7	287	104034	2.1	5.1037	1.6	14.4581	2.4	0.5352	1.8	0.75	2763.2	40.2	2780.3	22.7	2792.6	26.0	2792.6	26.0	98.9
RO346A-8	1151	53052	7.2	7.4431	2.4	6.5636	2.6	0.3543	0.9	0.36	1955.2	15.7	2054.5	22.8	2155.6	42.1	2155.6	42.1	90.7
RO346A-9	212	35336	1.4	8.4105	1.1	5.2967	1.9	0.3231	1.6	0.84	1804.8	25.2	1868.3	16.4	1939.7	18.8	1939.7	18.8	93.0
RO346A-10	187	49710	1.7	5.2472	0.9	13.8578	1.1	0.5274	0.7	0.64	2730.4	16.2	2740.0	10.8	2747.2	14.3	2747.2	14.3	99.4
RO346A-11	296	4300	2.5	10.5863	5.0	2.8097	5.1	0.2157	0.8	0.16	1259.3	9.4	1358.1	38.1	1517.4	94.6	1517.4	94.6	83.0
RO346A-12	1121	3090	3.2	5.2981	2.0	10.0024	4.4	0.3843	4.0	0.90	2096.5	70.7	2435.0	40.7	2731.3	32.1	2731.3	32.1	76.8
RO346A-13	1594	3742	7.3	7.8896	1.5	5.0298	4.7	0.2878	4.5	0.95	1630.6	64.1	1824.4	39.7	2053.3	25.8	2053.3	25.8	79.4
RO346A-14	458	5620	1.0	5.2583	2.0	11.4649	3.0	0.4372	2.2	0.74	2338.3	43.5	2561.7	28.1	2743.7	33.4	2743.7	33.4	85.2
RO346A-15	737	62646	4.1	4.5991	1.7	16.8161	2.2	0.5609	1.4	0.63	2870.4	32.9	2924.4	21.5	2961.8	28.1	2961.8	28.1	96.9
RO346A-16	582	16258	2.1	4.5630	1.2	16.1707	1.7	0.5352	1.2	0.72	2763.1	27.9	2886.9	16.5	2974.5	19.4	2974.5	19.4	92.9
RO346A-17	701	50560	2.9	4.8882	2.4	14.3866	3.3	0.5100	2.3	0.68	2656.8	49.2	2775.5	31.5	2863.0	39.5	2863.0	39.5	92.8
RO346A-19	1305	32410	5.0	5.1131	2.1	13.9226	3.1	0.5163	2.4	0.76	2683.5	52.0	2744.5	29.7	2789.6	33.6	2789.6	33.6	96.2
RO346A-20	634	13582	3.0	5.3350	1.2	12.6255	2.6	0.4885	2.4	0.90	2564.2	49.9	2652.1	24.8	2719.8	19.3	2719.8	19.3	94.3
RO346A-21	104	29132	1.3	5.6293	1.3	11.0668	3.1	0.4518	2.8	0.91	2403.4	56.2	2528.8	28.6	2631.0	20.9	2631.0	20.9	91.3
RO346A-22	1384	21890	9.1	7.7770	1.9	6.4676	2.9	0.3648	2.2	0.76	2004.9	37.6	2041.5	25.3	2078.7	33.0	2078.7	33.0	96.4
RO346A-23	451	20308	1.3	4.7461	2.1	16.1830	2.5	0.5571	1.3	0.54	2854.4	30.7	2887.7	23.5	2910.9	33.5	2910.9	33.5	98.1
RO346A-25	476	43890	1.8	4.6778	1.5	16.8803	2.7	0.5727	2.3	0.84	2918.9	54.0	2928.1	26.3	2934.4	24.3	2934.4	24.3	99.5
RO346A-27	134	11974	1.5	11.5070	1.6	2.7060	1.9	0.2258	1.0	0.54	1312.6	11.9	1330.1	13.7	1358.3	30.1	1358.3	30.1	96.6
RO346A-28	1161	3950	2.1	4.7048	1.7	13.6998	2.1	0.4675	1.3	0.59	2472.5	25.9	2729.2	20.1	2925.1	27.7	2925.1	27.7	84.5
RO346A-29	1411	172596	5.0	7.9893	1.5	6.2791	3.2	0.3638	2.8	0.89	2000.3	48.7	2015.5	28.0	2031.1	26.2	2031.1	26.2	98.5
RO346A-30	356	2288	6.5	14.5703	2.9	0.9999	3.0	0.1057	0.9	0.30	647.5	5.6	703.8	15.3	887.7	59.5	647.5	5.6	72.9
RO346A-31	1080	85836	4.1	8.2176	1.3	6.0350	1.6	0.3597	1.0	0.63	1980.7	17.6	1980.9	14.2	1981.1	22.4	1981.1	22.4	100.0
RO346A-32	719	2616	2.3	10.4598	1.5	3.0894	3.0	0.2344	2.6	0.87	1357.3	31.5	1430.1	22.7	1540.0	27.6	1540.0	27.6	88.1
RO346A-35	734	31956	22.0	7.9472	0.9	6.3633	1.1	0.3668	0.5	0.48	2014.2	8.6	2027.2	9.2	2040.5	16.3	2040.5	16.3	98.7
RO346A-37	699	13642	0.9	5.5503	1.9	10.9890	2.6	0.4424	1.8	0.67	2361.2	34.6	2522.2	24.2	2654.4	31.9	2654.4	31.9	89.0
RO346A-39	505	130966	1.4	4.6951	0.9	16.5292	1.6	0.5628	1.3	0.82	2878.4	29.7	2907.9	14.9	2928.4	14.2	2928.4	14.2	98.3
RO346A-40	158	8438	1.0	16.6338	2.2	0.8381	2.3	0.1011	0.8	0.34	620.9	4.7	618.1	10.7	607.8	47.2	620.9	4.7	102.2
RO346A-42	317	83696	2.3	4.7795	1.2	15.9764	2.1	0.5538	1.8	0.84	2841.0	40.9	2875.4	20.4	2899.5	19.0	2899.5	19.0	98.0
RO346A-43	1303	90288	17.9	5.3779	1.0	12.5162	1.7	0.4882	1.4	0.81	2562.8	29.4	2643.9	16.1	2706.6	16.5	2706.6	16.5	94.7
RO346A-45	756	102270	2.3	8.2539	0.7	5.5676	1.3	0.3333	1.1	0.83	1854.3	18.0	1911.1	11.6	1973.3	13.2	1973.3	13.2	94.0
RO346A-50	313	14132	3.0	16.0840	1.6	0.9425	2.7	0.1099	2.2	0.81	672.5	13.9	674.2	13.2	680.1	33.3	672.5	13.9	98.9
RO346A-51	474	13548	1.6	3.7752	1.3	24.2388	1.5	0.6637	0.8	0.53	3281.4	20.8	3278.0	15.0	3276.0	20.6	3276.0	20.6	100.2
RO346A-52	827	13848	0.9	4.6838	0.7	15.4344	2.5	0.5243	2.4	0.96	2717.4	53.4	2842.4	23.9	2932.3	10.9	2932.3	10.9	92.7
RO346A-53	111	13274	1.9	10.3794	1.2	3.6451	1.3	0.2744	0.6	0.48	1563.1	8.9	1559.4	10.6	1554.5	21.9	1554.5	21.9	100.6
RO346A-54	192	58866	1.1	3.7020	1.1	24.9232	1.2	0.6692	0.5	0.41	3302.7	12.9	3305.2	12.0	3306.7	17.6	3306.7	17.6	99.9
RO346A-46	286	17772	1.1	16.5728	1.6	0.8589	1.9	0.1032	0.9	0.48	633.4	5.4	629.5	8.8	615.8	35.5	633.4	5.4	102.9
RO346A-47	247	14632	1.2	16.0685	1.6	0.9910	1.9	0.1155	1.1	0.57	704.6	7.4	699.2	9.8	682.1	33.8	704.6	7.4	103.3
RO346A-48	568	2042	1.1	4.5709	1.8	15.8607	3.4	0.5258	2.9	0.86	2723.7	64.4	2868.4	32.4	2971.7	28.3	2971.7	28.3	91.7
RO346A-49	306	34328	2.5	11.6548	1.1	2.6913	1.4	0.2275	0.8	0.60	1321.3	9.8	1326.1	10.2	1333.7	21.3	1333.7	21.3	99.1
RO346A-55	568	62888	1.3	10.3260	1.3	3.6926	1.9	0.2765	1.4	0.74	1573.9	19.7	1569.8	15.3	1564.2	24.4	1564.2	24.4	100.6
RO346A-56	446	76356	7.9	7.3531	2.2	6.9562	2.3	0.3710	0.5	0.22	2034.0	8.9	2105.9	20.1	2176.8	38.5	2176.8	38.5	93.4
RO346A-58	1390	27010	3.0	5.1026	0.7	14.5236	1.2	0.5375	0.9	0.78	2772.9	20.7	2784.5	11.2	2793.0	12.1	2793.0	12.1	99.3
RO346A-59	1006	140816	2.0	10.5360	1.0	3.5244	1.8	0.2693	1.5	0.85	1537.3	21.1	1532.7	14.3	1526.3	17.9	1526.3	17.9	100.7
RO346A-60	520	104086	2.0	4.7132	0.7	16.5341	1.6	0.5652	1.5	0.91	2888.0	34.7	2908.2	15.8	2922.2	11.3	2922.2	11.3	98.8
RO346A-61	738	105970	10.9	8.0630	1.1	6.0749	1.2	0.3553	0.5	0.41	1959.6	8.4	1986.7	10.7	2014.9	19.9	2014.9	19.9	97.3
RO346A-62	323	20524	1.1	15.6170	1.8	1.0857	2.1	0.1230	1.1	0.52	747.6	7.8	746.4	11.1	742.7	37.8	747.6	7.8	100.7
RO346A-63	1242	2822	10.3	7.6785	1.1	5.9011	2.2	0.3286	2.0	0.88	1831.7	31.3	1961.4	19.4	2101.1	18.7	2101.1	18.7	87.2
RO346A-64	570	38348	4.0	6.6069	1.6	9.2092	3.0	0.4413	2.5	0.83	2356.4	48.8	2359.0	27.2	2361.3	28.0	2361.3	28.0	99.8

Analysis	Isotope ratios										Apparent ages (Ma)								
	U (ppm)	206Pb 204Pb	U/Th	206Pb* 207Pb*	± (%)	207Pb* 235U*	± (%)	206Pb* 238U	± (%)	error corr.	206Pb* 238U*	± (Ma)	207Pb* 235U	± (Ma)	206Pb* 207Pb*	± (Ma)	Best age (Ma)	± (Ma)	Conc (%)
RO346A-65	673	131874	15.6	5.0165	0.9	13.8032	2.2	0.5022	2.0	0.91	2623.3	42.7	2736.3	20.6	2820.8	14.7	2820.8	14.7	93.0
RO346A-67	879	116634	4.1	5.6344	1.8	11.8142	2.4	0.4828	1.6	0.68	2539.4	34.2	2589.8	22.5	2629.5	29.3	2629.5	29.3	96.6
RO346A-68	1211	181212	5.5	8.2298	1.2	6.0765	2.2	0.3627	1.8	0.84	1994.9	31.2	1986.9	18.8	1978.5	20.7	1978.5	20.7	100.8
RO346A-69	287	41402	1.9	7.6939	1.8	6.7528	2.3	0.3768	1.4	0.61	2061.4	25.1	2079.6	20.4	2097.6	32.0	2097.6	32.0	98.3
RO346A-70	802	18028	5.0	7.5673	2.1	6.5405	3.3	0.3590	2.6	0.77	1977.3	43.9	2051.4	29.4	2126.7	37.2	2126.7	37.2	93.0
RO346A-71	570	53424	6.2	4.8219	1.8	15.2078	2.7	0.5318	2.0	0.73	2749.2	43.9	2828.3	25.4	2885.2	29.4	2885.2	29.4	95.3
RO346A-72	269	28568	0.7	4.6291	2.1	17.3811	4.2	0.5835	3.7	0.87	2963.2	87.7	2956.1	40.6	2951.3	33.3	2951.3	33.3	100.4
RO346A-74	533	30580	2.2	4.7053	1.3	16.8550	2.1	0.5752	1.6	0.78	2929.1	37.7	2926.6	19.8	2924.9	21.0	2924.9	21.0	100.1
RO346A-76	609	92374	3.4	8.1049	1.6	6.1760	1.7	0.3630	0.5	0.30	1996.6	8.6	2001.1	14.5	2005.7	28.1	2005.7	28.1	99.5
RO346A-77	1434	2764	3.1	7.7243	2.2	5.9664	2.7	0.3342	1.6	0.60	1858.9	25.8	1971.0	23.3	2090.7	37.8	2090.7	37.8	88.9
RO346A-78	533	7386	0.4	10.8835	1.3	2.9088	1.6	0.2296	1.0	0.61	1332.4	11.8	1384.2	12.1	1464.9	24.0	1464.9	24.0	91.0
RO346A-80	689	38866	84.4	5.5206	0.5	12.6579	0.9	0.5068	0.8	0.83	2643.0	16.3	2654.5	8.5	2663.3	8.3	2663.3	8.3	99.2
RO346A-81	104	19886	1.5	7.5723	2.0	7.2327	2.4	0.3972	1.4	0.57	2156.2	24.7	2140.5	21.3	2125.5	34.5	2125.5	34.5	101.4
RO346A-84	634	3012	2.5	3.8784	1.5	18.5408	2.2	0.5215	1.6	0.74	2705.6	35.6	3018.2	20.9	3233.6	23.0	3233.6	23.0	83.7
RO346A-87	687	138384	3.7	7.4487	1.0	7.3849	1.1	0.3990	0.5	0.45	2164.2	9.2	2159.1	10.0	2154.3	17.5	2154.3	17.5	100.5
RO346A-88	229	47390	1.2	7.6791	0.6	6.9418	0.9	0.3866	0.7	0.78	2107.1	12.4	2104.0	7.9	2101.0	9.8	2101.0	9.8	100.3
RO346A-89	561	7218	3.5	5.5289	1.5	10.6410	2.5	0.4267	2.0	0.79	2290.8	38.0	2492.3	23.2	2660.8	25.5	2660.8	25.5	86.1
RO346A-90	840	4988	2.6	15.1693	2.7	1.0632	3.0	0.1170	1.3	0.43	713.1	8.7	735.4	15.6	803.9	56.2	713.1	8.7	88.7
RO346A-91	116	928	1.0	12.8743	5.6	1.0338	6.2	0.0965	2.5	0.41	594.0	14.2	720.8	31.8	1138.6	112.2	594.0	14.2	52.2
RO346A-92	639	4786	1.2	4.9241	1.8	12.2191	3.5	0.4364	3.0	0.86	2334.4	59.0	2621.4	32.9	2851.1	29.4	2851.1	29.4	81.9
RO346A-93	433	20060	1.1	16.0438	1.3	0.9762	1.4	0.1136	0.5	0.35	693.6	3.3	691.7	7.1	685.4	28.3	693.6	3.3	101.2
RO346A-94	903	1930	3.7	5.9537	2.5	8.4874	3.2	0.3665	2.0	0.63	2012.8	34.6	2284.6	28.9	2537.4	41.4	2537.4	41.4	79.3
RO346A-95	326	65088	1.0	8.8137	2.1	5.1212	2.3	0.3274	1.1	0.46	1825.6	16.9	1839.6	19.7	1855.5	37.2	1855.5	37.2	98.4
RO346A-96	748	70814	5.4	5.1399	1.6	11.6110	2.1	0.4328	1.2	0.60	2318.5	24.1	2573.6	19.2	2781.1	26.9	2781.1	26.9	83.4
RO346A-97	203	2130	1.2	4.2114	8.0	17.7673	8.2	0.5427	1.9	0.23	2794.7	43.6	2977.2	79.4	3103.0	128.0	3103.0	128.0	90.1
RO346A-98	514	78698	83.8	7.8857	1.6	6.3008	2.0	0.3604	1.2	0.60	1983.9	20.7	2018.6	17.7	2054.2	28.6	2054.2	28.6	96.6
RO346A-99	661	3662	1.3	4.5399	1.7	14.5870	2.7	0.4803	2.1	0.78	2528.6	44.3	2788.7	26.0	2982.6	27.8	2982.6	27.8	84.8
RO346A-100	277	112176	1.3	5.0295	2.0	14.8504	2.0	0.5417	0.5	0.25	2790.6	11.3	2805.7	19.2	2816.6	31.9	2816.6	31.9	99.1
RO346A-102	360	89738	1.2	7.7045	1.2	6.5719	1.6	0.3672	1.1	0.66	2016.3	18.7	2055.6	14.5	2095.2	21.8	2095.2	21.8	96.2
RO346A-103	357	16838	4.0	12.1018	3.6	2.2120	11.3	0.1941	10.8	0.95	1143.8	112.9	1184.8	79.5	1260.5	69.8	1260.5	69.8	90.7
RO346A-104	315	16552	2.7	15.8338	2.2	1.0420	2.4	0.1197	1.0	0.41	728.6	7.0	724.9	12.7	713.5	47.3	728.6	7.0	102.1
RO346B-1	455	122086	2.9	4.4740	2.6	18.5214	2.8	0.6010	1.1	0.38	3033.8	25.7	3017.2	26.6	3006.2	41.0	3006.2	41.0	100.9
RO346B-2	441	142574	2.5	10.7155	1.3	3.2890	2.5	0.2556	2.2	0.86	1467.4	28.9	1478.5	19.8	1494.4	24.2	1494.4	24.2	98.2
RO346B-3	97	20186	1.0	10.6595	1.4	3.2768	1.9	0.2533	1.4	0.70	1455.6	17.9	1475.6	15.2	1504.3	26.2	1504.3	26.2	96.8
RO346B-4	312	5112	2.0	15.3902	2.9	1.0097	6.0	0.1127	5.3	0.88	688.4	34.5	708.7	30.7	773.6	60.1	688.4	34.5	89.0
RO346B-5	371	22052	1.9	5.2766	0.8	13.8453	3.9	0.5298	3.9	0.98	2740.8	86.0	2739.2	37.3	2738.0	13.5	2738.0	13.5	100.1
RO346B-6	1024	66816	2.9	5.0319	3.2	14.5489	5.5	0.5310	4.5	0.81	2745.5	99.9	2786.2	52.4	2815.8	52.6	2815.8	52.6	97.5
RO346B-7	48	7058	1.7	12.2148	3.8	1.8462	4.1	0.1636	1.5	0.38	976.5	14.0	1062.1	27.0	1242.4	74.4	1242.4	74.4	78.6
RO346B-8	371	136426	2.2	5.2119	1.7	13.8414	1.9	0.5232	0.8	0.45	2712.8	18.6	2738.9	17.5	2758.2	27.1	2758.2	27.1	98.4
RO346B-9	347	143734	5.6	4.9107	14.3	15.1791	14.5	0.5406	2.0	0.14	2786.0	44.3	2826.5	138.7	2855.5	234.8	2855.5	234.8	97.6
RO346B-10	199	6980	0.8	5.3138	2.8	12.9234	3.5	0.4981	2.1	0.61	2605.4	45.9	2674.1	33.1	2726.4	45.8	2726.4	45.8	95.6
RO346B-11	287	15566	4.5	5.1526	1.4	13.9859	1.6	0.5227	0.8	0.47	2710.4	16.6	2748.8	15.1	2777.0	23.0	2777.0	23.0	97.6
RO346B-12	580	125266	2.2	4.6687	1.5	15.6379	3.3	0.5295	2.9	0.89	2739.4	65.6	2854.9	31.7	2937.5	24.9	2937.5	24.9	93.3
RO346B-13	888	44828	15.6	6.6022	2.1	8.4842	2.3	0.4063	1.0	0.42	2197.8	18.1	2284.2	21.2	2362.5	36.2	2362.5	36.2	93.0
RO346B-14	247	43404	4.7	12.5956	2.3	1.7657	3.1	0.1613	2.1	0.67	964.0	18.5	1033.0	20.1	1182.0	45.7	1182.0	45.7	81.6
RO346B-15	152	66200	2.2	5.4744	1.6	12.6575	1.8	0.5026	0.7	0.42	2624.8	16.0	2654.5	16.7	2677.2	26.6	2677.2	26.6	98.0
RO346B-16	549	38116	2.1	16.3533	1.6	0.9424	2.2	0.1118	1.5	0.68	683.1	9.6	674.2	10.7	644.5	34.0	683.1	9.6	106.0
RO346B-17	283	105996	1.8	5.2483	1.0	13.9835	2.2	0.5323	1.9	0.88	2751.0	42.3	2748.6	20.4	2746.8	17.1	2746.8	17.1	100.2
RO346B-18	309	6710	1.9	13.3094	4.5	1.7186	4.8	0.1659	1.5	0.31	989.4	13.4	1015.5	30.6	1072.1	91.2	1072.1	91.2	92.3
RO346B-19	404	112472	4.6	8.0824	1.1	6.0291	1.2	0.3534	0.5	0.42	1950.9	8.4	1980.1	10.3	2010.6	19.0	2010.6	19.0	97.0
RO346B-20	513	53706	3.0	4.7923	1.8	14.5482	2.0	0.5056	0.9	0.46	2638.0	19.9	2786.2	19.1	2895.2	29.0	2895.2	29.0	91.1

Analysis	Isotope ratios										Apparent ages (Ma)								
	U (ppm)	206Pb 204Pb	U/Th	206Pb* 207Pb*	± (%)	207Pb* 235U*	± (%)	206Pb* 238U	± (%)	error corr.	206Pb* 238U*	± (Ma)	207Pb* 235U	± (Ma)	206Pb* 207Pb*	± (Ma)	Best age (Ma)	± (Ma)	Conc (%)
RO346B-21	317	149518	1.8	5.3220	1.2	13.4774	1.7	0.5202	1.2	0.69	2700.1	25.4	2713.7	15.8	2723.9	20.1	2723.9	20.1	99.1
RO346B-22	163	48180	1.8	7.7160	1.0	6.6501	1.5	0.3722	1.2	0.77	2039.5	20.3	2066.0	13.3	2092.5	16.9	2092.5	16.9	97.5
RO346B-23	264	132296	2.4	4.6979	0.9	15.7992	1.0	0.5383	0.5	0.50	2776.4	11.3	2864.7	9.5	2927.5	13.9	2927.5	13.9	94.8
RO346B-24	303	1414	2.4	5.0184	3.1	13.2880	3.2	0.4836	0.7	0.22	2543.1	14.5	2700.3	29.8	2820.2	50.2	2820.2	50.2	90.2
RO346B-25	166	67394	1.2	5.4226	1.3	12.2551	1.4	0.4820	0.5	0.36	2535.8	10.5	2624.1	13.0	2693.0	21.3	2693.0	21.3	94.2
RO346B-26	821	16838	3.0	7.8400	3.0	6.3353	3.7	0.3602	2.3	0.61	1983.3	38.4	2023.4	32.6	2064.5	52.1	2064.5	52.1	96.1
RO346B-27	605	1038	3.5	5.0722	4.2	12.6406	4.3	0.4650	0.9	0.21	2461.6	18.5	2653.2	40.4	2802.8	68.7	2802.8	68.7	87.8
RO346B-28	371	149692	1.7	5.0085	0.7	14.5413	1.4	0.5282	1.3	0.88	2733.9	28.1	2785.7	13.6	2823.4	11.1	2823.4	11.1	96.8
RO346B-29	414	171456	1.9	4.5639	1.0	17.6582	1.4	0.5845	1.0	0.70	2967.0	23.8	2971.3	13.7	2974.2	16.3	2974.2	16.3	99.8
RO346B-30	172	14286	1.6	16.6057	1.9	0.7919	2.4	0.0954	1.4	0.58	587.2	7.7	592.2	10.7	611.5	41.8	587.2	7.7	96.0
RO346B-32	188	20142	2.0	15.2119	3.2	0.8897	4.0	0.0982	2.4	0.60	603.6	14.0	646.2	19.3	798.0	67.5	603.6	14.0	75.6
RO346B-33	471	98782	1.8	4.6290	1.0	16.9390	1.1	0.5687	0.5	0.44	2902.4	11.7	2931.4	11.0	2951.3	16.6	2951.3	16.6	98.3
RO346B-34	554	134868	4.3	4.1277	1.0	19.4910	1.2	0.5835	0.6	0.50	2963.0	13.8	3066.4	11.2	3134.9	16.1	3134.9	16.1	94.5
RO346B-36	728	29796	9.1	8.1635	1.3	5.8740	2.1	0.3478	1.6	0.77	1924.0	26.8	1957.4	18.1	1992.9	23.7	1992.9	23.7	96.5
RO346B-37	221	7720	1.6	4.5037	1.9	17.7791	2.1	0.5807	0.7	0.35	2951.7	17.3	2977.9	19.8	2995.5	31.0	2995.5	31.0	98.5
RO346B-38	804	20272	10.1	5.4886	3.8	11.4046	5.1	0.4540	3.4	0.66	2413.0	67.6	2556.8	47.5	2672.9	63.1	2672.9	63.1	90.3
RO346B-39	603	187422	2.0	4.6112	1.5	15.4949	1.6	0.5182	0.6	0.37	2691.5	13.4	2846.2	15.5	2957.5	24.4	2957.5	24.4	91.0
RO346B-40	434	539318	3.9	5.4100	1.6	11.8061	1.8	0.4632	0.9	0.49	2453.8	18.2	2589.1	17.1	2696.8	26.4	2696.8	26.4	91.0
RO346B-41	1161	95484	7.0	5.1950	1.1	12.6805	2.4	0.4778	2.1	0.89	2517.6	44.6	2656.2	22.6	2763.6	17.7	2763.6	17.7	91.1
RO346B-42	427	37024	1.0	5.4230	1.2	11.4063	2.9	0.4486	2.6	0.91	2389.1	52.5	2556.9	27.1	2692.8	20.2	2692.8	20.2	88.7
RO346B-44	1052	111164	2.1	7.7973	0.7	6.7249	1.5	0.3803	1.3	0.89	2077.7	23.3	2075.9	13.0	2074.1	11.6	2074.1	11.6	100.2
RO346B-45	792	4496	7.9	5.2914	2.6	11.9716	3.3	0.4594	2.0	0.60	2437.1	39.6	2602.2	30.5	2733.3	42.8	2733.3	42.8	89.2
RO346B-46	555	155318	4.0	5.2161	0.9	13.7112	1.1	0.5187	0.5	0.47	2693.7	11.0	2730.0	10.1	2756.9	15.4	2756.9	15.4	97.7
RO346B-47	1063	69540	12.0	16.3747	0.8	0.8479	1.0	0.1007	0.6	0.59	618.5	3.4	623.5	4.5	641.7	16.8	618.5	3.4	96.4
RO346B-48	497	32892	4.9	4.9644	1.1	14.0757	1.2	0.5068	0.5	0.45	2642.9	11.7	2754.8	11.3	2837.8	17.3	2837.8	17.3	93.1
RO346B-49	66	49484	2.4	5.5781	1.3	11.7124	2.0	0.4738	1.5	0.77	2500.4	31.9	2581.7	18.8	2646.1	21.4	2646.1	21.4	94.5
RO346B-50	450	95272	3.8	4.7993	1.1	15.0027	1.2	0.5222	0.5	0.43	2708.5	11.1	2815.4	11.2	2892.9	17.2	2892.9	17.2	93.6
RO346B-51	362	152056	3.7	13.5705	1.4	1.7258	1.5	0.1699	0.6	0.36	1011.3	5.1	1018.2	9.9	1032.9	29.1	1032.9	29.1	97.9
RO346B-52	651	26474	6.9	5.6521	2.1	10.7964	2.9	0.4426	2.0	0.70	2362.1	40.0	2505.8	26.9	2624.3	34.4	2624.3	34.4	90.0
RO346B-54	219	8376	2.5	6.3096	2.1	9.1548	2.6	0.4189	1.5	0.59	2255.6	29.1	2353.6	23.6	2439.6	35.2	2439.6	35.2	92.5
RO346B-55	668	53584	3.5	4.5708	1.0	17.4965	1.1	0.5800	0.5	0.44	2948.8	11.8	2962.5	11.0	2971.7	16.6	2971.7	16.6	99.2
RO346B-56	249	104828	1.8	5.3530	1.5	13.3706	1.6	0.5191	0.5	0.32	2695.3	11.0	2706.2	14.7	2714.3	24.2	2714.3	24.2	99.3
RO346B-57	587	13506	1.4	4.5156	1.6	18.1969	3.2	0.5960	2.8	0.87	3013.5	67.6	3000.2	31.2	2991.3	26.1	2991.3	26.1	100.7
RO346B-58	83	25026	2.2	5.2663	2.3	13.3034	2.4	0.5081	0.6	0.27	2648.6	13.9	2701.4	22.3	2741.2	37.4	2741.2	37.4	96.6
RO346B-59	2671	3518	6.0	5.0298	1.5	14.8105	2.5	0.5403	2.1	0.81	2784.6	46.4	2803.1	24.1	2816.5	24.2	2816.5	24.2	98.9
RO346B-60	509	58766	2.6	5.1977	1.3	14.0359	1.5	0.5291	0.8	0.53	2737.7	18.1	2752.1	14.5	2762.7	21.3	2762.7	21.3	99.1
RO346B-61	171	26296	1.6	9.4962	0.8	4.3000	2.1	0.2962	2.0	0.93	1672.2	28.7	1693.4	17.4	1719.6	14.6	1719.6	14.6	97.2
RO346B-62	430	116280	5.7	4.8083	0.8	15.3630	1.4	0.5358	1.2	0.81	2765.7	25.9	2838.0	13.5	2889.8	13.5	2889.8	13.5	95.7
RO346B-63	1113	142540	7.3	8.2226	0.8	5.6288	2.6	0.3357	2.5	0.96	1865.8	40.7	1920.5	22.6	1980.1	13.5	1980.1	13.5	94.2
RO346B-64	259	109474	2.3	5.3534	0.7	12.9969	0.8	0.5046	0.5	0.59	2633.6	10.8	2679.4	8.0	2714.2	11.2	2714.2	11.2	97.0
RO346B-65	694	142432	3.1	4.7141	1.1	16.8025	2.7	0.5745	2.4	0.91	2926.2	56.9	2923.6	25.4	2921.9	17.5	2921.9	17.5	100.1
RO346B-66	585	153648	1.6	4.6201	0.9	17.0448	1.0	0.5711	0.5	0.50	2912.5	12.0	2937.4	9.8	2954.4	14.4	2954.4	14.4	98.6
RO346B-67	249	23256	2.2	9.6378	1.2	4.3377	2.4	0.3032	2.1	0.88	1707.2	31.6	1700.6	19.9	1692.4	21.4	1692.4	21.4	100.9
RO346B-68	640	29344	3.3	4.6646	1.7	16.4465	2.2	0.5564	1.5	0.65	2851.7	33.6	2903.1	21.5	2938.9	27.6	2938.9	27.6	97.0
RO346B-69	549	48798	2.0	15.7291	1.1	1.0380	1.4	0.1184	0.9	0.62	721.4	6.1	722.9	7.5	727.6	24.0	721.4	6.1	99.2
RO346B-70	414	159878	3.0	5.3407	1.2	13.1053	1.7	0.5076	1.3	0.74	2646.5	27.6	2687.3	16.2	2718.1	19.1	2718.1	19.1	97.4
RO346B-73	668	158892	2.2	4.5803	1.0	17.4082	1.2	0.5783	0.7	0.60	2941.8	17.5	2957.6	11.8	2968.4	15.8	2968.4	15.8	99.1
RO346B-74	350	61964	2.6	5.9792	1.2	9.6970	1.3	0.4205	0.5	0.38	2262.8	9.5	2406.4	12.2	2530.3	20.7	2530.3	20.7	89.4
RO346B-75	282	109500	2.0	4.6236	0.6	16.9480	1.4	0.5683	1.3	0.90	2900.9	29.2	2931.9	13.3	2953.2	9.8	2953.2	9.8	98.2
RO346B-77	627	153464	3.0	4.9330	0.7	14.6917	0.9	0.5256	0.6	0.60	2723.0	12.2	2795.5	8.8	2848.2	12.1	2848.2	12.1	95.6
RO346B-78	810	150102	21.2	16.5232	1.6	0.8396	2.0	0.1006	1.2	0.60	618.0	7.1	618.9	9.3	622.2	34.6	618.0	7.1	99.3
RO346B-79	209	21408	4.7	16.1772	2.2	0.9755	2.7	0.1145	1.6	0.58	698.6	10.3	691.3	13.5	667.7	47.1	698.6	10.3	104.6

Analysis	Isotope ratios										Apparent ages (Ma)								
	U (ppm)	206Pb 204Pb	U/Th	206Pb* 207Pb*	± (%)	207Pb* 235U*	± (%)	206Pb* 238U	± (%)	error corr.	206Pb* 238U*	± (Ma)	207Pb* 235U	± (Ma)	206Pb* 207Pb*	± (Ma)	Best age (Ma)	± (Ma)	Conc (%)
RO346B-80	131	21224	3.6	12.4922	1.3	2.2578	1.9	0.2046	1.4	0.71	1199.8	14.8	1199.2	13.4	1198.2	26.5	1198.2	26.5	100.1
RO346B-81	522	162948	1.9	4.6135	1.2	17.5040	2.2	0.5857	1.9	0.85	2971.9	44.3	2962.9	21.0	2956.7	18.6	2956.7	18.6	100.5
RO346B-82	724	54746	2.0	4.6153	0.9	16.9957	1.7	0.5689	1.5	0.86	2903.3	33.9	2934.6	16.1	2956.1	13.7	2956.1	13.7	98.2
RO346B-83	192	44068	1.1	10.8140	1.1	3.2223	2.1	0.2527	1.7	0.84	1452.5	22.4	1462.5	15.9	1477.1	21.3	1477.1	21.3	98.3
RO346B-84	261	91216	2.4	16.4757	2.7	0.8796	3.0	0.1051	1.3	0.43	644.2	7.9	640.8	14.4	628.4	59.1	644.2	7.9	102.5
RO346B-85	975	228464	2.7	8.1036	0.7	6.1387	1.3	0.3608	1.1	0.85	1985.9	19.3	1995.8	11.6	2006.0	12.4	2006.0	12.4	99.0
RO346B-86	187	17526	2.6	16.8174	2.8	0.7772	3.2	0.0948	1.5	0.48	583.8	8.5	583.9	14.1	584.0	60.3	583.8	8.5	100.0
RO346B-87	242	27638	1.3	16.0007	1.9	0.9350	3.3	0.1085	2.7	0.82	664.1	16.9	670.3	16.0	691.2	39.8	664.1	16.9	96.1
RO346B-89	679	4538	4.9	5.5248	2.3	11.0642	2.5	0.4433	0.9	0.36	2365.6	18.0	2528.6	23.3	2662.1	38.5	2662.1	38.5	88.9
RO346B-90	307	64314	1.5	10.8324	1.4	3.2981	1.7	0.2591	1.0	0.57	1485.3	12.6	1480.6	13.0	1473.9	26.0	1473.9	26.0	100.8
RO346B-91	637	142240	2.5	5.3672	0.8	13.1880	1.2	0.5134	0.8	0.72	2671.0	18.2	2693.2	10.9	2709.9	13.4	2709.9	13.4	98.6
RO346B-92	432	168452	1.8	4.6509	1.1	16.4387	1.4	0.5545	0.8	0.59	2843.9	18.6	2902.7	13.1	2943.7	17.8	2943.7	17.8	96.6
RO346B-93	207	19600	2.6	5.4168	1.0	12.3240	1.2	0.4842	0.7	0.58	2545.4	14.5	2629.4	11.1	2694.7	15.9	2694.7	15.9	94.5
RO346B-94	456	20212	3.6	5.0375	1.4	14.9515	1.7	0.5463	1.0	0.56	2809.6	22.1	2812.2	16.5	2814.0	23.4	2814.0	23.4	99.8
RO346B-96	240	47558	2.7	5.3965	1.3	12.7229	1.6	0.4980	0.9	0.59	2605.0	20.1	2659.4	15.1	2700.9	21.5	2700.9	21.5	96.4
RO346B-97	258	156290	6.1	5.3401	1.6	12.9518	1.7	0.5016	0.6	0.34	2620.8	12.9	2676.2	16.5	2718.2	27.0	2718.2	27.0	96.4
RO346B-98	204	34852	1.9	10.7089	0.8	3.2607	1.4	0.2533	1.2	0.84	1455.2	15.8	1471.7	11.2	1495.6	14.6	1495.6	14.6	97.3
RO346B-99	286	103250	3.1	4.7099	1.1	15.7586	1.2	0.5383	0.6	0.49	2776.3	13.5	2862.3	11.6	2923.3	17.2	2923.3	17.2	95.0
RO346B-100	365	251238	4.8	4.5947	0.9	16.8466	1.8	0.5614	1.6	0.86	2872.4	36.2	2926.1	17.4	2963.3	14.8	2963.3	14.8	96.9
RO346B-101	173	6730	1.9	15.4416	2.9	0.8520	3.4	0.0954	1.9	0.55	587.5	10.7	625.8	16.1	766.5	60.5	587.5	10.7	76.6
RO346B-102	1015	44766	4.5	5.4074	2.0	13.2773	2.6	0.5207	1.6	0.61	2702.2	34.4	2699.6	24.2	2697.6	33.5	2697.6	33.5	100.2
RO346B-103	197	19776	1.3	17.1184	2.6	0.7628	3.0	0.0947	1.5	0.51	583.3	8.5	575.6	13.1	545.4	55.9	583.3	8.5	106.9
RO346B-104	143	30524	1.7	10.6288	1.7	3.3411	2.1	0.2576	1.3	0.61	1477.3	17.0	1490.7	16.5	1509.8	31.6	1509.8	31.6	97.9
RO346B-105	568	114030	3.8	4.6486	1.4	16.5163	2.3	0.5568	1.8	0.80	2853.6	41.5	2907.2	21.7	2944.5	22.1	2944.5	22.1	96.9

All uncertainties are reported at the 1-sigma level, and include only measurement errors. Systematic errors would increase age uncertainties by 1–2 %. U concentration and U/Th are calibrated relative to our Sri Lanka standard zircon, and are accurate to ~20 %. Common Pb correction is from ^{204}Pb, with composition interpreted from Stacey & Kramers (1975) and uncertainties of 1.0 for $^{206}Pb/^{204}Pb$, 0.3 for $^{207}Pb/^{204}Pb$, and 2.0 for $^{208}Pb/^{204}Pb$. U/Pb and $^{206}Pb/^{207}Pb$ fractionation is calibrated relative to fragments of a large Sri Lanka zircon of 564±4 Ma (2-sigma). U decay constants and composition as follows: $^{238}U = 9.8485\times10^{-10}$, $^{235}U = 1.55125\times10^{-10}$, $^{238}U/^{235}U = 137.88$